OXFORD

Modeling gain-of-function and loss-of-function components of *SPAST*-based hereditary spastic paraplegia using transgenic mice

Emanuela Piermarini[1], Seyma Akarsu[1,2], Theresa Connors[1], Matthias Kneussel[3], Michael A. Lane[1], Gerardo Morfini[4],

Arzu Karabay [2], Peter W. Baas[1,†,*] and Liang Qiang [1,†,*]

[1]Department of Neurobiology and Anatomy, Drexel University College of Medicine, Philadelphia, PA 19129, USA
[2]Department of Molecular Biology and Genetics, Istanbul Technical University, Istanbul 34469, Turkey
[3]Department of Molecular Neurogenetics, Center for Molecular Neurobiology, ZMNH, University Medical Center Hamburg-Eppendorf, Hamburg 20251, Germany
[4]Department of Anatomy and Cell Biology, University of Illinois at Chicago, Chicago, IL 60612, USA
*To whom correspondence should be addressed at: Drexel University College of Medicine, 2900 Queen Lane, Philadelphia, PA 19129, USA. Tel: +1 2159918311;
Fax: +1 2158439082; Email: lq24@drexel.edu; Tel: +1 2159918298; Email: pwb22@drexel.edu

[†]Equal contributions, co-Senior Authors.

Abstract

Hereditary spastic paraplegia (HSP) is a disease in which dieback degeneration of corticospinal tracts, accompanied by axonal swellings, leads to gait deficiencies. *SPG4*-HSP, the most common form of the disease, results from mutations of human spastin gene (*SPAST*), which is the gene that encodes spastin, a microtubule-severing protein. The lack of a vertebrate model that recapitulates both the etiology and symptoms of *SPG4*-HSP has stymied the development of effective therapies for the disease. h*SPAST*-C448Y mice, which express human mutant spastin at the *ROSA26* locus, display corticospinal dieback and gait deficiencies but not axonal swellings. On the other hand, mouse spastin gene (*Spast*)-knockout (KO) mice display axonal swellings but not corticospinal dieback or gait deficiencies. One possibility is that reduced spastin function, resulting in axonal swellings, is not the cause of the disease but exacerbates the toxic effects of the mutant protein. To explore this idea, *Spast*-KO and h*SPAST*-C448Y mice were crossbred, and the offspring were compared with the parental lines via histological and behavioral analyses. The crossbred animals displayed axonal swellings as well as earlier onset, worsened gait deficiencies and corticospinal dieback compared with the h*SPAST*-C448Y mouse. These results, together with observations on changes in histone deacetylases 6 and tubulin modifications in the axon, indicate that each of these three transgenic mouse lines is valuable for investigating a different component of the disease pathology. Moreover, the crossbred mice are the best vertebrate model to date for testing potential therapies for *SPG4*-HSP.

Introduction

Hereditary spastic paraplegia (HSP) is a heritable neurodegenerative disorder, usually adult onset, in which spasticity with progressive muscle weakness of the lower limbs leads to gait deficiencies (1). These gait deficiencies result from dieback degeneration of the corticospinal tracts (CSTs) during which the relevant axons display pathological swellings along their length (2). Human spastin gene (*SPAST*), the most commonly mutated gene in HSP, encodes spastin, a microtubule (MT)-severing protein with membrane-related properties. Mutations in *SPAST* result in an autosomal dominant form of the disease called *SPG4*-HSP. Progress has been slow in developing therapies for patients with *SPG4*-HSP, in part because of the lack of a vertebrate model that recapitulates both the etiology and symptoms of the disease.

On the presumption of haploinsufficiency as the etiology of the disease, cellular and animal models for *SPG4*-HSP for many years revolved around the partial or complete knockdown of expression of the endogenous spastin genes (3–6). This presumption was based on the lack of detection of mutant spastin proteins in non-neuronal cells and tissues from human patients (7,8) and the fact that the same disease is produced by different pathogenic mutations of *SPAST* that vary in type, including missense, nonsense, frameshift and truncating (9). To this day, most experimental data in the field are still interpreted within the framework of haploinsufficiency, as are most clinical studies on patients. Curiously, however, the corticospinal axons in mouse spastin gene (*Spast*)-knockout (KO) mice display swellings, but they neither display dieback degeneration nor gait deficiencies (10–12).

Challenging the presumption of haploinsufficiency, studies from our laboratories have provided evidence for a gain-of-function etiology for *SPG4*-HSP. These studies, conducted on various cellular and invertebrate model systems, have shown that when spastin is mutated, one of its two isoforms, termed M1, acquires cytotoxic

properties not shared by the other isoform, termed M87 (M85 in rodents) (9,13–15). M1 accumulates in the spinal cord but not in non-neuronal cells or tissues, potentially explaining the lack of detection of mutant spastin proteins in those earlier studies. Building on this work, we recently generated a new mouse model, termed h*SPAST*-C448Y, in which full-length human spastin with the missense C448Y mutation was inserted into the *ROSA26* locus (16). This mouse, which also expresses the normal complement of functional mouse spastin, displays adult-onset gait deficiencies and corticospinal dieback degeneration but no axonal swellings (16).

Taking these various observations into account, we have proposed that cytotoxicity of mutant spastin proteins is necessary and sufficient for corticospinal dieback degeneration and gait deficiencies but that reduced spastin function renders the axons more vulnerable to the toxic effects of the mutant proteins (17). In this scenario, the axonal swellings are a morphological indicator of this vulnerability. If this scenario is correct, both the h*SPAST*-C448Y and the *Spast*-KO mouse are useful in that they isolate for study one of the two key components of the disease, namely gain-of-function of the mutant spastin or loss-of-function of wild-type spastin. However, crossbreeding the two mouse lines should theoretically produce offspring that recapitulate both components of the disease, with axonal swellings as well as dieback degeneration and gait defects that are exacerbated compared with the h*SPAST*-C448Y. If this is the case, the crossbred animals would be to date the most accurate vertebrate model for testing potential therapies for the disease. Here, we explore this scenario and also expand our studies on the mechanistic basis of the disease by exploring potential changes in post-translational tubulin acetylation resulting from each component of the disease.

Results

Generation of h*SPAST*-C448Y$^{+/-}$;*Spast*$^{+/-}$ (dHet) mouse model

A transgenic mouse model with a full-length human spastin carrying the missense mutation C448Y was crossed with a *Spast*-KO mouse (Fig. 1A). Briefly, a floxed (loxP-flanked) transcriptional STOP cassette was incorporated between the transgene and the promoter to allow expression to be dependent upon Cre recombinase. Ubiquitous Cre mice obtained from GenOway were used to unlock the expression of the mutant spastin (16). The *Spast*-KO mouse (named *Spast*$^-$) (18) was generated via the KO-first approach. As a result, deletion of *Spast* expression was achieved, and mice were genotyped by polymerase chain reaction (PCR). Genomic DNA (gDNA) obtained from ear punches of the offspring were used to identify genotypes (Fig. 1B). Semi-quantitative PCR was performed to identify *Spast*$^{+/-}$ heterozygotes (see primer pairs for distinguishing either the wild-type allele or the KO allele, Fig. 1C and D), while quantitative real-time PCR

(qRT-PCR) was applied to verify the expression of C448Y-mutated human spastin (see primer pair for identifying the h*SPAST* insert at the ROSA 26 locus, Fig. 1E and F). Heterozygous mice from both lines were crossbred, and typical PCR genotyping results are shown in Figure 1C–F.

The double heterozygous (h*SPAST*-C448Y$^{+/-}$;*Spast*$^{+/-}$) mouse was confirmed by qPCR to contain one allele of human *SPAST*-C448Y (at ROSA26 locus) and one null allele of mouse spastin. Moreover, western blot analysis on spinal cord tissues from hemi-/heterozygous adult mice confirmed the expected reductions in spastin levels in *Spast*$^{+/-}$ and in both h*SPAST*-C448Y$^{+/-}$ and h*SPAST*-C448Y$^{+/-}$;*Spast*$^{+/-}$. Of note, the latter two both displayed accumulated levels of M1 (Fig. 1G and H). Heterozygous mice were used for these analyses since *SPG4-HSP* is an autosomal dominant disease. Therefore, the following genotypes were applied to this study: wild-type, *Spast*$^{+/-}$, h*SPAST*-C448Y$^{+/-}$ and h*SPAST*-C448Y$^{+/-}$; *Spast*$^{+/-}$. The four genotypes are referred to as wild-type, m-KO-Het, h-KI-Het and dHet, respectively. Thus, for the first time, a mouse model in which functional spastin is reduced together with the expression of human mutated spastin was created.

Gait impairments relevant to human HSP symptoms identified in dHet mice and h-KI-Het mice, but not in m-KO-Het mice, also exacerbated in dHet mice

One of the most objective and sensitive assays for gait deficiencies and locomotor malfunctions in rodent models is the Catwalk automated quantitative gait analysis, a computer-assisted assay capable of detecting even very subtle motor abnormalities (Fig. 2A and B) (19–22). Longitudinal analyses were performed on a cohort of four different genotypes: wild-type, m-KO-Het, h-KI-Het and dHet, all of which were tested at different ages as 2, 3, 6, 9, 12 and 15 months of age. To assess potential behavior deficits, 8–12 animals were used for each genotype at different ages of life. Animals underwent a week of training to learn the task before recording (Fig. 2C).

All of our behavioral studies were carried out on males because our previous studies indicated that males maintain a more consistent and severe phenotype compared with their female counterparts (16). Among all of the parameters that can be extracted from the recorded movies, a subset of parameters was selected based on their close relevance to the gait defects observed in HSP patients (23). No obvious defects during development were observed in any of the four groups. All of the mice were retired from further testing at 15 months of age. The parameters included in the study are (i) stand duration, (ii) swing duration, (iii) step width, (iv) base of support and (v) paw prints position (Figs 2 and 3). Paw prints are obviously not included in human studies (23) but are important for evaluating gait impairment in rodents.

No significant differences were identified in animals younger than 3 months of age regarding any of the parameters examined (>25 out of 100), including
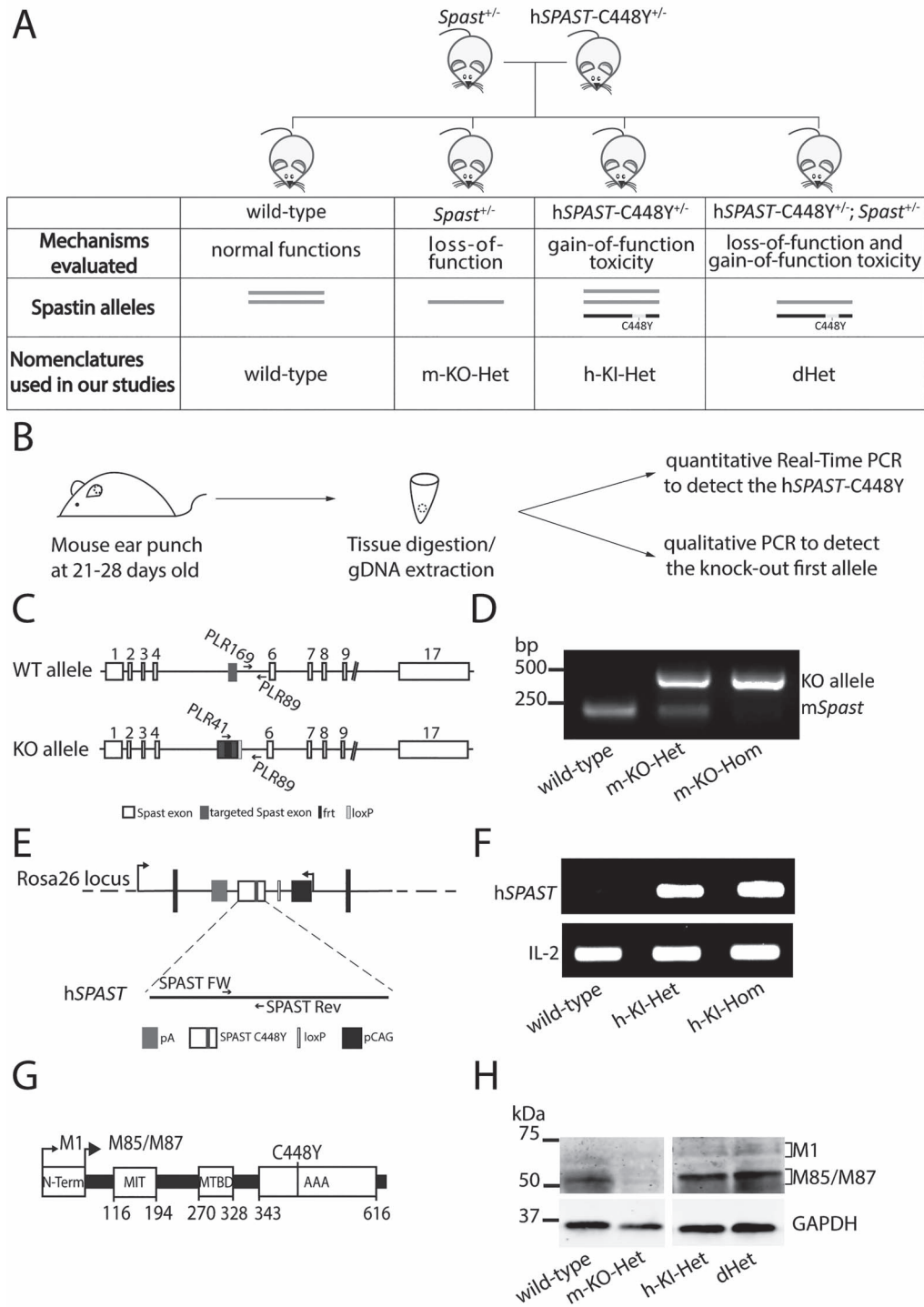
Figure 1. Generation of the mouse models of four genotypes for the study of SPG4-HSP etiology. (**A**) The strategy used to generate mouse models of the four genotypes. *Spast*$^{+/-}$ and hSPAST-C448Y$^{+/-}$ mice were crossbred to obtain the four genotypes of interest: the hSPAST-C448Y$^{-/-}$;*Spast*$^{+/+}$ mice (aka wild-type) have normal functions and two endogenous mouse spastin alleles; the *Spast*$^{+/-}$ mice (aka m-KO-Het) have a loss-of-function phenotype and one endogenous mouse spastin allele; the hSPAST-C448Y$^{+/-}$ mice (aka h-KI-Het) have a gain-of-function toxicity phenotype with one human mutated spastin allele with the two endogenous mouse spastin alleles. The hSPAST-C448Y$^{+/-}$;*Spast*$^{+/-}$ mice (aka dHet) have both loss-of-function and gain-of-function phenotypes and they possess one human-mutated C448Y allele and one mouse endogenous spastin allele. (**B**) Mice were ear punched at 21–28 days of age and gDNA was extracted to perform qRT-PCRs and qualitative PCRs to validate their genotypes. (**C**) Schematic representation of the primers annealing on the mouse *Spast* sequence. (**D**) gDNA was subjected to a touchdown PCR protocol to discriminate wild-type and *Spast*-KO mice, both heterozygous (m-KO-Het) and homozygous (m-KO-Hom), among the littermates. (**E**) Schematic representation of the primers annealing on the human *SPAST* sequence. (**F**) gDNA products from qRT-PCR were electrophoresed on 1% agarose gel to visualize the hSPAST band among the three genotypes in the transgenic hSPAST-C448Y mouse model: wild-type, heterozygous (h-KI-Het) and homozygous (h-KI-Hom). (**G**) Schematic illustration of spastin protein domains. M1 and M85/M87 start codons are highlighted. N-Term, N-terminal; MIT, microtubules interacting and trafficking domain; MTBD, microtubule binding domain; AAA, ATPase associated with various cellular activities. The localization of the C448Y mutation is also shown at the AAA domain. (**H**) A representative western blotting image of distinct spastin expression patterns in the spinal cord tissues in all four genotypes of interest.
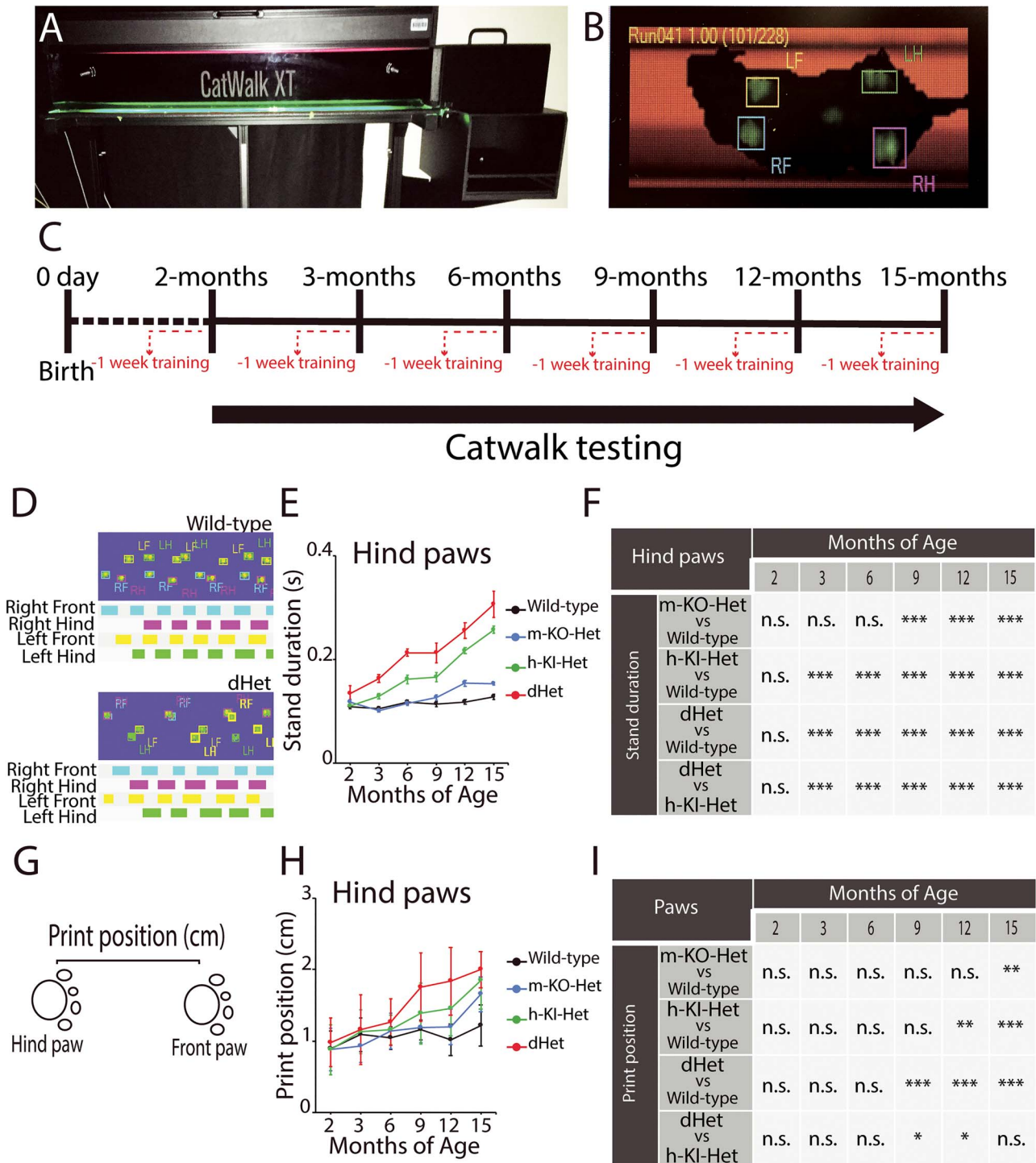
Figure 2. Timeline and parameters of Catwalk analyses applied to identify the gait impairments related to *SPG4-HSP*. (**A**) The Catwalk apparatus is shown. (**B**) Each movie required a post-processing step to obtain all of the parameters for the subsequent analysis. (**C**) The timeline shows the age points taken for analysis of each of the four groups. One week prior the actual recording, mice were trained for the task. (**D**) Representative timing view of wild-type and dHet paws during recording. (**E** and **F**) Stand duration of the hind paws shows significant increase in h-KI-Het mice during adulthood. The phenotype is worsened in dHet mouse model. (**G**) The print position measures the distance between the position of the hind paw and the previously placed front paw on the same side of the body and in the same step cycle. (**H** and **I**) Print position parameter shows a significant increase in h-KI-Het, which is more prominent in dHet mice. Between 8 and 12 animals were used for the behavioral testing, and data are represented as mean ± S.D. For statistical tests, one-way ANOVA with Tukey *post hoc* analysis was conducted. *$P < 0.05$, **$P < 0.002$, ***$P < 0.001$. For additional information related to this figure, see Tables 1 and 2.

the most relevant 5 listed before among all of the 4 mouse groups (Figs 2 and 3). Gait impairment started to appear in certain mouse groups when they reached 3 months of age. Both h-KI-Het and dHet mice showed prolonged stand durations that affected mainly the hind paws (Fig. 2D–F, Table 1), while no significant differences were detected for the front paws (Supplementary Material, Fig. S1A and B, Supplementary Material, Table S1).
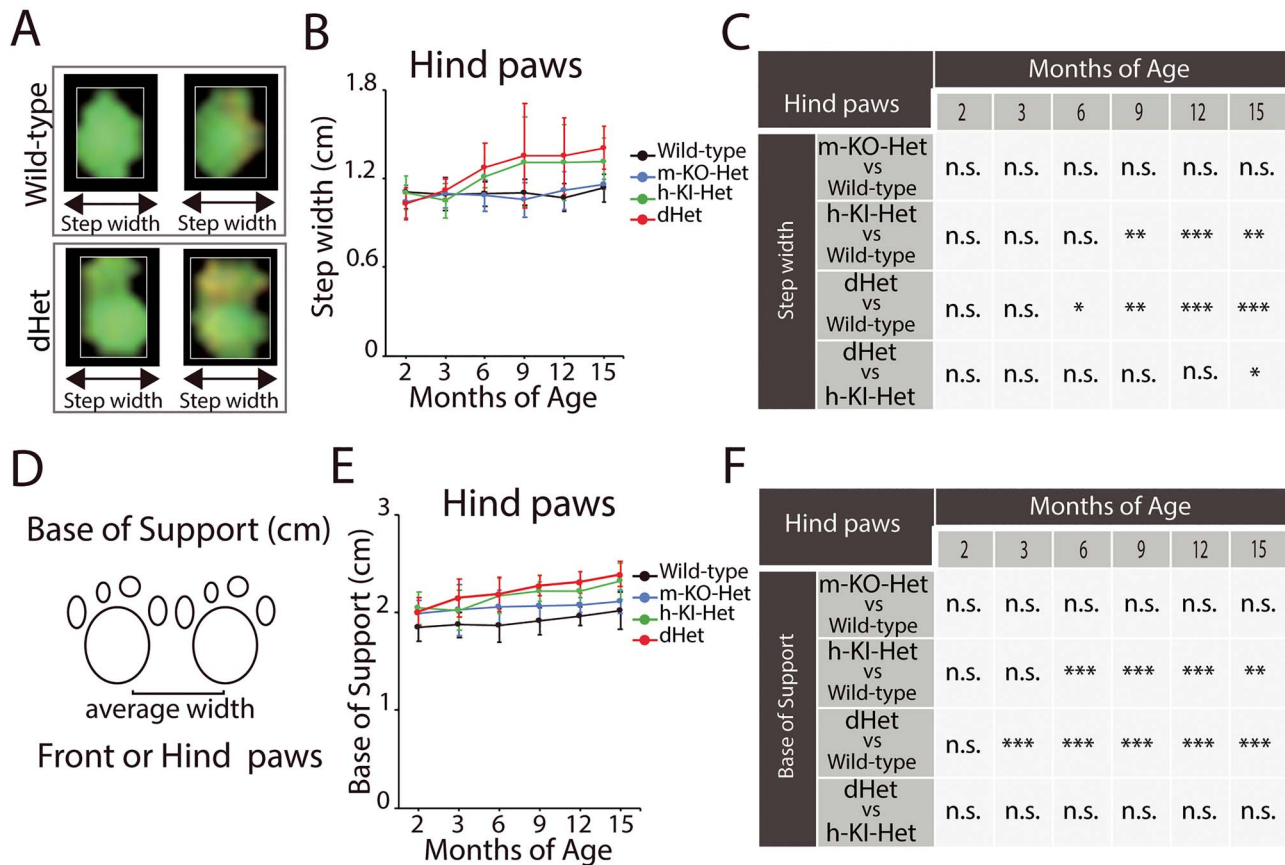
Figure 3. Step width and base of support in the Catwalk analyses among the mice with all four genotypes. (**A**) Representative step width paws of wild-type and dHet. (**B** and **C**) Hind paws step width significantly increase in h-KI-Het at 9 months of age. Symptoms for this parameter appeared earlier in dHet at 6 months of age, highlighting a stronger phenotype compared with h-KI-Het. (**D**) The base of support represents the average width in cm between either the front paws or the hind paws. (**E** and **F**) The hind paw base of support highlights a significant change in h-KI-Het, which is more prominent in the dHet mice starting at 3 months of age. Between 8 and 12 animals were used for the behavioral testing, and data are represented as mean ± S.D. For statistical tests, one-way ANOVA with Tukey *post hoc* analysis was conducted. *$P < 0.05$, **$P < 0.002$, ***$P < 0.001$. For additional information related to this figure, see Tables 3 and 4.

Significant differences were also observed for the print position parameter (Fig. 2G) in the case of the h-KI-Het and the dHet, compared with the control mice, whereas no such differences were identified in m-KO-Het (Fig. 2H and I, Table 2). Increased step width (Fig. 3A) was also detected in both h-KI-Het and dHet in the hind paws, with a significant increase around 6 months of age (Fig. 3B and C, Table 3) that became worse in dHet compared with h-KI-Het at 15 months of age; while no significant differences were found in the front paws among the four genotypes (Supplementary Material, Fig. S1C and D, Supplementary Material, Table S2). Moreover, an increased base of support (Fig. 3D) in the hind paws was found in h-KI-Het and dHet mice (Fig. 3E and F, Table 4). No significant differences for this parameter were detected in the front paws (Supplementary Fig. 1E and F, Supplementary Material, Table S3).

Consistent with our hypothesis, compared with h-KI-Het, the double transgenic dHet mice manifested significantly deteriorated phenotypes in those parameters. To ascertain whether m-KO-Het mice display any gait deficiencies at ≥3 months of age, we exhausted the measurements on 20 more different parameters that can

be extracted from the database of our Catwalk analyses. No significant differences were detected in any of the parameters between m-KO-Het and wild-type control (data not shown). Evidence from our longitudinal Catwalk analyses showed that dHet mice displayed worse gait deficiencies than the h-KI-Het mouse, which were manifested in stand duration, step width, base of support and print position, although both mice showed pathological differences compared with the wild-type control (Figs 2 and 3). No significant differences were detected among any of the four mouse groups for the swing duration parameter (Supplementary Material, Fig. S2, Supplementary Material, Tables S4 and S5).

Distinct axonal defects identified in h-KI-Het, m-KO-Het and dHet mice

SGP4-HSP is thought to be primarily caused by the degeneration of the upper motor neurons whose cell bodies reside in the motor cerebral cortex, with their long axons projecting into the spinal cord to form the CSTs (24,25). Previously, we applied different experimental strategies that showed consistent anatomical evidence of dieback

Table 1. Stand duration of the hind paws

Hind paws stand duration	Wild-type (s)	m-KO-Het (s)	h-KI-Het (s)	dHet (s)
2 months	0.110 ± 0.005	0.117 ± 0.005	0.111 ± 0.004	0.134 ± 0.015
3 months	0.105 ± 0.004	0.101 ± 0.003	0.129 ± 0.005	0.163 ± 0.008
6 months	0.118 ± 0.003	0.116 ± 0.004	0.162 ± 0.008	0.213 ± 0.007
9 months	0.114 ± 0.005	0.127 ± 0.005	0.166 ± 0.009	0.213 ± 0.019
12 months	0.118 ± 0.005	0.154 ± 0.006	0.217 ± 0.006	0.256 ± 0.015
15 months	0.128 ± 0.005	0.153 ± 0.002	0.257 ± 0.007	0.306 ± 0.025

Table 2. Print position

Print position	Wild-type (cm)	m-KO-Het (cm)	h-KI-Het (cm)	dHet (cm)
2 months	0.891 ± 0.250	0.882 ± 0.295	0.879 ± 0.350	0.981 ± 0.339
3 months	1.087 ± 0.233	0.926 ± 0.226	1.131 ± 0.304	1.159 ± 0.490
6 months	1.040 ± 0.158	1.140 ± 0.252	1.156 ± 0.207	1.264 ± 0.328
9 months	1.155 ± 0.142	1.189 ± 0.212	1.383 ± 0.425	1.753 ± 0.476
12 months	1.012 ± 0.220	1.194 ± 0.249	1.454 ± 0.381	1.836 ± 0.475
15 months	1.215 ± 0.284	1.653 ± 0.244	1.849 ± 0.402	1.996 ± 0.254

Table 3. Step width of the hind paws

Hind paws step width	Wild-type (cm)	m-KO-Het (cm)	h-KI-Het (cm)	dHet (cm)
2 months	1.108 ± 0.110	1.041 ± 0.111	1.101 ± 0.113	1.027 ± 0.108
3 months	1.094 ± 0.111	1.097 ± 0.096	1.050 ± 0.118	1.123 ± 0.077
6 months	1.095 ± 0.081	1.085 ± 0.104	1.209 ± 0.072	1.275 ± 0.167
9 months	1.106 ± 0.090	1.055 ± 0.116	1.310 ± 0.305	1.352 ± 0.352
12 months	1.071 ± 0.095	1.119 ± 0.128	1.309 ± 0.256	1.352 ± 0.261
15 months	1.136 ± 0.094	1.159 ± 0.033	1.313 ± 0.158	1.407 ± 0.146

Table 4. Base of Support of the hind paws

Hind paws base of support	Wild-type (cm)	m-KO-Het (cm)	h-KI-Het (cm)	dHet (cm)
2 months	1.851 ± 0.143	1.986 ± 0.141	2.043 ± 0.163	2.005 ± 0.143
3 months	1.872 ± 0.131	2.025 ± 0.258	2.021 ± 0.203	2.150 ± 0.194
6 months	1.868 ± 0.169	2.060 ± 0.172	2.169 ± 0.178	2.189 ± 0.175
9 months	1.911 ± 0.140	2.069 ± 0.148	2.217 ± 0.101	2.272 ± 0.104
12 months	1.961 ± 0.096	2.077 ± 0.074	2.215 ± 0.121	2.311 ± 0.108
15 months	2.017 ± 0.188	2.112 ± 0.119	2.318 ± 0.185	2.391 ± 0.129

axonal degeneration in the CSTs of the h-KI-Het mouse (16). Based on the results obtained from the previous Catwalk analyses, we sought to examine whether phenotypical dieback degeneration of CSTs is worse in the dHet mouse than that in the h-KI-Het mouse. We also inquired as to whether any anatomical changes could be identified in the m-KO-Het mouse, although no overt gait impairment was detected in the Catwalk analyses. Because our previous data using multiple experimental methods for anatomical examination all led to a similar conclusion, we decided to select one of them to proceed, which was to compare the axon morphologies and numbers between the cervical and lumbar level in the spinal cord via toluidine blue staining (16). The majority of the CSTs locates in the ventral portion of the dorsal column in the spinal cord (>95%) (26), which was the region of interest in our studies.

We measured and compared axonal numbers and perimeter from the spinal cord at both cervical and lumbar levels by carrying out toluidine blue staining on semi-thin plastic embedded cross-sections of all the four mouse groups, as illustrated in Figure 4A. Our initial set of analyses was made on the tissues of mice that were 2 months of age (Fig. 4B); no significant differences were found in axonal numbers among the four groups (Fig. 4C and D, Table 5). We then examined these parameters in the mice at 6 months of age, when significant gait impairments were detected in the h-KI-Het and dHet mice. Axonal counts at cervical and lumbar levels (Fig. 4E and F) revealed a significant reduction in both h-KI-Het and dHet mice compared with their wild-type counterparts at the lumbar level, whereas no such reduction was detected in m-KO-Het mice (Fig. 4G and H, Table 6). Both h-KO-Het and

Table 5. Total axon count on 2-month-old mice

Axon count per μm^2	Cervical level	Lumbar level
Wild-type	1.479 ± 0.454	1.271 ± 0.138
m-KO-Het	1.216 ± 0.200	1.291 ± 0.183
h-KI-Het	1.310 ± 0.144	1.122 ± 0.307
dHet	1.376 ± 0.194	1.253 ± 0.207

Table 6. Total axon count on 6-month-old mice

Axon count per μm^2	Cervical level	Lumbar level
Wild-type	1.130 ± 0.114	1.679 ± 0.454
m-KO-Het	1.217 ± 0.298	1.216 ± 0.200
h-KI-Het	1.270 ± 0.232	0.610 ± 0.144
dHet	1.036 ± 0.126	0.759 ± 0.194

Table 7. Number of axons in mice at 6 months of age

Axon count per μm^2	Normal axons	Swollen axons
Wild-type	1.410 ± 0.153	0.270 ± 0.119
m-KO-Het	0.290 ± 0.183	0.920 ± 0.221
h-KI-Het	0.420 ± 0.126	0.200 ± 0.105
dHet	0.540 ± 0.149	0.480 ± 0.115

Table 8. Axon perimeter in a cross-section (μm) in mice at 6 months of age

	Axon perimeter in a cross-section (μm)
Wild-type	1.233 ± 0.773
m-KO-Het	3.975 ± 1.238
h-KI-Het	1.022 ± 0.348
dHet	3.518 ± 0.638

Table 9. Total axon count in mice at 15 months of age

Axon count per μm^2	Cervical level	Lumbar level
Wild-type	1.879 ± 0.454	2.194 ± 0.475
m-KO-Het	1.616 ± 0.300	1.857 ± 0.370
h-KI-Het	1.710 ± 0.144	1.153 ± 0.249
dHet	1.676 ± 0.395	0.687 ± 0.202

dHet mice showed a significant increase in axonal perimeter, suggesting axonal swellings occur in those mice in adulthood, whereas no such differences were detected in h-KI-Het mice, which express the mutant human spastins with the normal functional spastin level (Fig. 4I and J, Tables 7 and 8). At 15 months of age, tissues from wild-type, m-KO-Het, h-KI-Het and dHet revealed a more drastic phenotype; the h-KI-Het and dHet showed a severely reduced number of axons occurred at this old stage of their life, as shown in Figure 4K and L and Table 9.

Reduced MT acetylation and increased histone deacetylases 6 activity in spinal cords of dHet and h-KI-Het mice but not m-KO-Het mice

Previously, decreased MT acetylation was documented in the spinal cord of the h-KI-Het mouse (16), and other findings consistent with reduced MT stability were reported in various experimental models involving mutant spastins (13,27). This is especially interesting because the inverse is expected when spastin levels or activity are reduced, given that spastin preferentially severs MTs in their more stable regions, and this is what has been observed in cultured rodent neurons with experimentally reduced spastin (28). In mice with both haploinsufficiency and gain-of-function toxicity, the question arises as to which of these effects predominates. In pursuing MT acetylation, we also explored MT detyrosination, which is a separate modification of tubulin that occurs on the stable regions of MTs. For reasons that are unknown, changes in MT acetylation or detyrosination often result in corresponding changes in the other (29,30). We assessed MT acetylation as a ratio of acetylated to total tubulin, and we indirectly assessed MT detyrosination as a ratio of tyrosinated to total tubulin.

Spinal cord tissues from the wild-type, m-KO-Het, h-KI-Het and dHet mice were collected for western blotting analyses using antibodies against acetylated or tyrosinated tubulin. No differences in the amount of βIII-tubulin were observed across the four genotypes (Fig. 5A and B). Strikingly, compared with wild-type, the levels of tyrosinated tubulin were significantly increased in both h-KI-Het and dHet mice, whereas a decrease was observed in m-KO-Het mice (Fig. 5A and C). As shown previously (16), significantly reduced levels of acetylated tubulin were found in h-KI-Het mice (Fig. 5A and D), while no change in acetylated tubulin was observed in m-KO-Het mice (Fig. 5A and D). More interestingly, the levels of acetylated MTs in dHet mice were as reduced as they were in h-KI-Het (Fig. 5A and D), which negates the possibility that the two effects offset one another. Rather, it appears that the tubulin modification response to the gain-of-function toxic mechanisms overrides the opposite effect of the haploinsufficiency. In fact, the data trend toward the deacetylation and tyrosination in the crossbred mouse being potentially even worsened.

In neuronal cytoplasm, histone deacetylases 6 (HDAC6), a member of type II HDACs, is the chief deacetylase responsible for removing the acetyl group from Lys40 of α-tubulin within MTs (31). As such, its levels/activities are an important regulator of MT acetylation in axons. Unlike most of the other HDACs, which are localized within the nucleus, HDAC6 concentrates in cytoplasm owing to the presence of a nuclear export sequence and a serine-glutamate-containing tetrapeptide motif (SE14), which ensures its stable cytoplasmic retention (32). To assess HDAC6 activities in different mouse models, a fluorometric-based measurement was used on spinal cord tissues from wild-type, m-KO-Het, h-KI-Het and
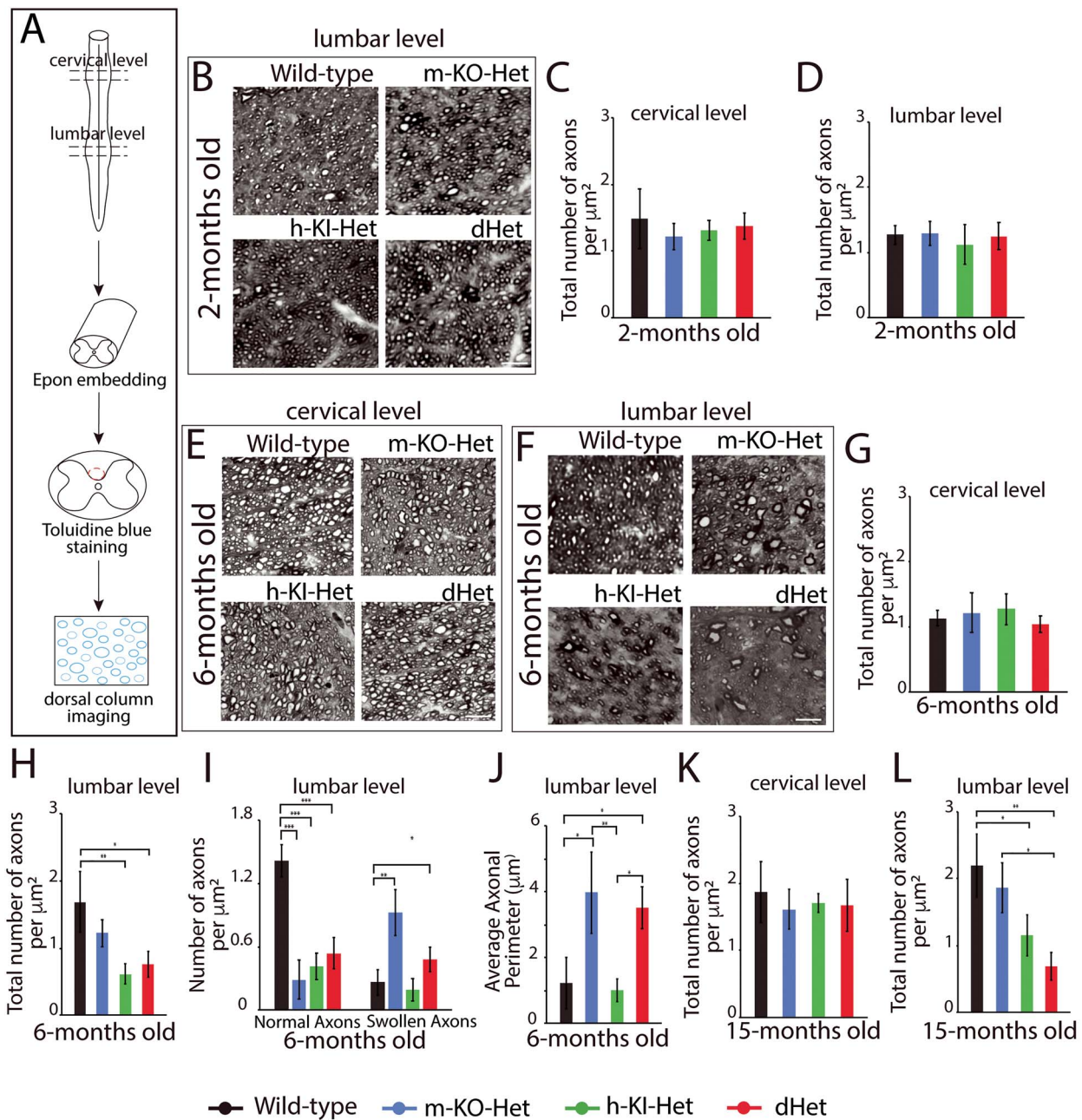
Figure 4. Distinct axon defects identified in the dorsal columns of the spinal cords in m-KO-Het, h-KI-Het and dHet mice. (**A**) The schematic illustrates the methodology used to study axonal morphology. Spinal cords were dissected at cervical and lumbar levels, embedded in epon, and semi-thin 1 μm sections were obtained. Images of dorsal columns were taken with phase contrast optics for subsequent analysis. (**B**) Zoomed toluidine blue-stained images of the dorsal columns at the lumbar level of mice at 2 months of age were used to count the number of axons. (**C**) Cervical and (**D**) lumbar level analyses show no significant differences among the four groups in the axonal counts at 2 months of age. Representative images of (**E**) cervical and (**F**) lumbar level of the four groups at 6 months of age. (**G**) Cervical level shows no significant change in mice at 6 months of age. (**H**) Total axonal counts at the lumbar level show a drastic decrease in axonal number in h-KI-Het and dHet. (**I**) Axons were classified according to their shape as normal or swollen. The analysis revealed a significant increase in swollen axons in m-KO-Het and dHet. (**J**) The average perimeter of axons was also considered. A significant increase in axonal perimeter was detected in both m-KO-Het and dHet. Mice at 15 months of age were also analyzed for the axonal count. (**K**) At the cervical level, no significant differences were revealed. (**L**) Total number of axons at the lumbar level reveals a significant decrease of axons in h-KI-Het and dHet. Data are represented as mean ± S.D. For statistical tests, one-way ANOVA with Tukey *post hoc* analysis was conducted. Scale bar in (B, E and F): 10 μm. *$P < 0.05$, **$P < 0.002$, ***$P < 0.001$. For additional information related to this figure, see Tables 5–9.

dHet mice. No significant changes were observed in the HDAC6 activities between wild-type and m-KO-Het mice (Fig. 5E). However, significantly enhanced HDAC6 activities were found in the spinal cords of both h-KI-Het and dHet mice; this provides a potential explanation for the lowered MT acetylation in the spinal cords of these animals (Fig. 5E).

Discussion

SPG4-HSP, despite being the most common form of HSP, is a rare disease and hence progress has been slow in elucidating its etiology. Attention on *SPG4*-HSP intensified when it was discovered that spastin is a MT-severing protein (33), with the assumption in the field
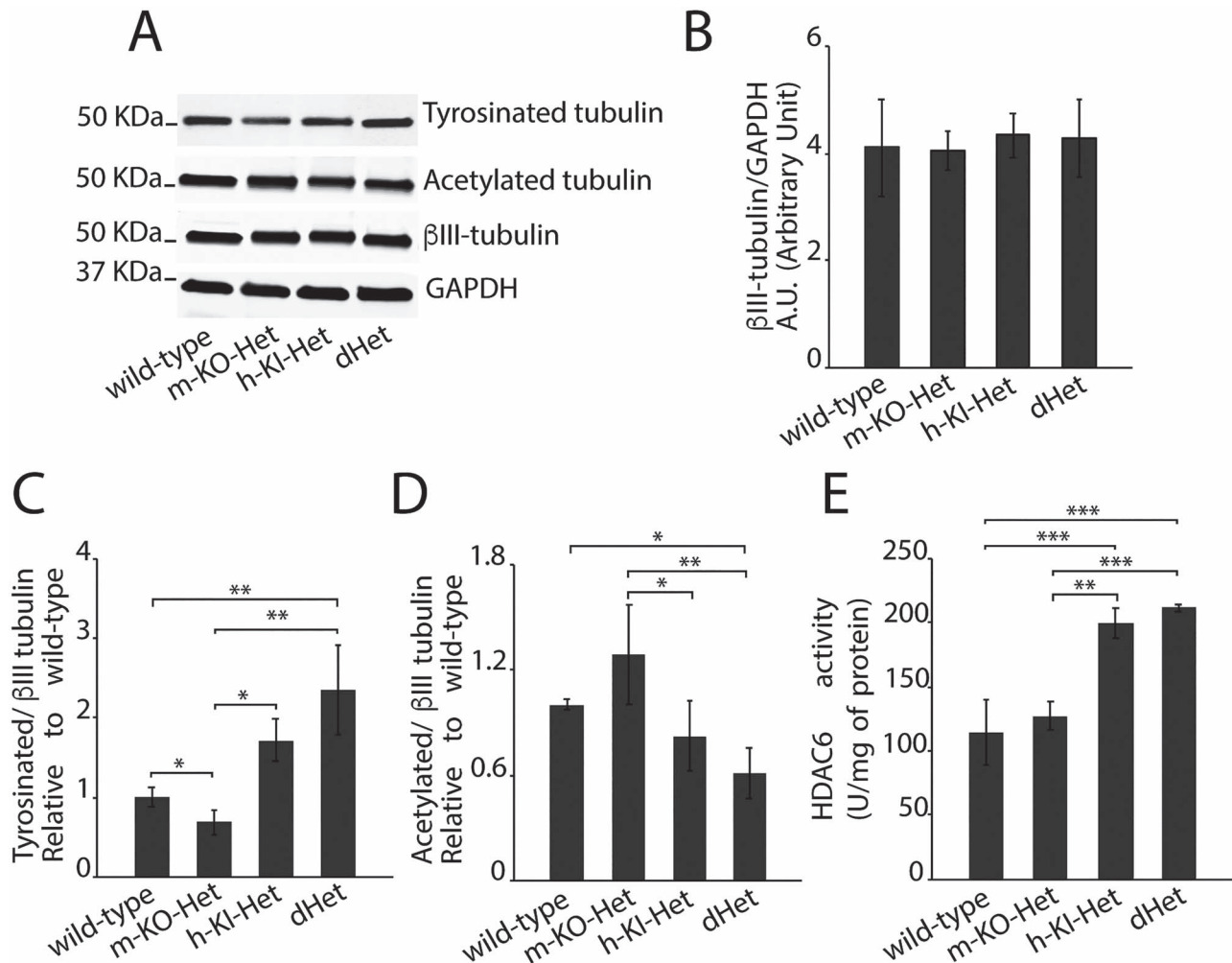
Figure 5. Altered tubulin acetylation and HDAC6 activity in h-KI-Het and dHet mice but not in m-KO-Het mice. (**A**) Representative western blots of lower spinal cord immunoblotted for acetylated-, tyrosinated- and βIII-tubulin. (**B**) βIII-tubulin shows no significant changes across the four groups when normalized to GAPDH. (**C** and **D**) All the western blot analyses for tyrosinated and acetylated tubulin were ratioed to βIII-tubulin. (C) Analysis of tyrosinated tubulin revealed significant changes in the expression level at lower spinal cords for h-KI-Het and dHet mice, with expression levels at 1 ± 0.12, 0.69 ± 0.16, 1.72 ± 0.27 and 2.36 ± 0.56 for wild-type, m-KO-Het, h-KI-Het and dHet, respectively. (D) Analysis for acetylated tubulin revealed a decrease at the lower spinal cord for h-KI-Het and dHet, with expression levels at 1 ± 0.03, 1.28 ± 0.28, 0.82 ± 0.20 and 0.61 ± 0.15 for wild-type, m-KO-Het, h-KI-Het and dHet, respectively. (**E**) HDAC6 activity was measured from tissue lysates of lower spinal cords among the four groups. The assay was carried out according to manufacturer's instructions, the graph shows HDAC6 activity (U/mg of protein) $\pm$ S.D. Western blot and HDAC6 lysates were collected from three mice for each genotype. For statistical tests, one-way ANOVA with Tukey *post hoc* analysis was conducted. *$P < 0.05$, **$P < 0.002$, ***$P < 0.001$.

being that the corticospinal degeneration in the disease results from insufficient spastin activity. However, the lack of corticospinal dieback and gait deficiency in spastin deficient mice called into question whether haploinsufficiency is, in fact, the sole component of the etiology. The prominent axonal swellings in the tracts appeared to be the only feature of these animals which recapitulated an aspect of the disease phenotype observed in human patients. In our own studies on cultured cells and invertebrate models, we were initially dismissive of haploinsufficiency (27), but a growing body of evidence has since suggested that spastin dosage is crucial to the normal vitality of neurons (34). On this basis, we recently posited that reduced spastin function may serve as a vulnerability factor not capable of causing the disease on its own but potentially able to render the CSTs more vulnerable to the toxicity of the mutant spastins.

Over the years, we have presented various lines of evidence that mutant M1 spastin is cytotoxic, for example, causing defects in axonal transport and abnormal organelle distribution (13,35). Our best evidence came from the hSPAST-C448Y mouse, which we designed not to be haploinsufficient while expressing a human mutant form of spastin (16). This animal showed adult-onset corticospinal dieback degeneration and gait deficiencies, remarkably similar to SPG4-HSP patients. Here, to test our hypothesis that haploinsufficiency might be an exacerbating factor, we crossbred the hSPAST-C448Y mouse with a Spast-KO mouse. The latter displayed axonal swellings, but no corticospinal degeneration and no gait deficiencies as revealed by the Catwalk assay, despite showing some unrelated motor and cognitive deficiencies in a previous study (18). The crossbred animals displayed all of the same features as the hSPAST-C448Y mouse, but stronger and earlier onset, and with

axonal swellings. These results lend support to the view that the axonal swellings are a morphological manifestation of the axon's greater vulnerability to the pathological mechanisms that cause the axonal dieback.

Collectively, these findings suggest that, depending on where they are in the progression of the disease, patients may benefit from therapies that address either the gain-of-function toxicity or haploinsufficiency component of the disease. For example, some patients do not suffer symptoms until late in life and hence staving off the effects of the haploinsufficiency may be sufficient to provide them quality of life, especially if the treatments that address the toxicity have harsher side-effects. Similarly, treatments for the toxicity, while more directly aimed at the etiology of the disease, may require time to work and hence the patient may benefit from pretreatment or co-treatment with therapies targeting haploinsufficiency. Moving forward, we will be interested in learning more about both aspects of the disease and developing appropriate therapies for each.

We previously reported that MT deacetylation is a consistent repercussion of the gain-of-function toxicity of mutant M1 spastin (16). However, experimental reduction of spastin levels has been reported to have the opposite effect, which is to increase MT acetylation (28). This latter effect owes to the fact that spastin preferentially severs MTs in their more stable/acetylated regions and hence lowering spastin activity leads to a greater fraction of the MTs being stable/acetylated. However, this had never been explored in KO mice, and our present results do not indicate a substantial reduction in MT acetylation, perhaps because of compensatory mechanisms (8). The crossbred mice also showed no less MT acetylation than the h*SPAST*-C448Y mice. This was also reflected in changes in at least one other tubulin modification (namely detyrosination) that, like acetylation, reflects the stability properties of axonal MTs. Such tubulin modifications are important regulators of the MT's interactions with various proteins, such as molecular motors, and hence may be critically important to corticospinal degeneration (36–38). For the first time, we documented an increase in HDAC6 activity, which is the major tubulin deacetylase in neurons, as a result of the expression of human mutant spastin, which provides a potential explanation for the decrease in tubulin acetylation. HDAC6 has been considered as a potential therapeutic target for other neurodegenerative disorders (39–42) and may serve in this capacity for *SPG4*-HSP as well.

Gain-of-function effects of misfolded proteins may exaggerate a normal function of the protein, for example, by exposing and making constitutively active an otherwise tightly regulated domain or might cause toxicity by a novel mechanism unrelated to the protein's normal function (43–45). We previously reported that mutant M1 spastin hyperactivates casein kinase 2 (CK2) which in turn reduces axonal transport by abnormally phosphorylating certain molecular motor proteins (13). The enhanced HDAC6 activity reported here may or may not relate to CK2, and whether either one, alone or in combination, causes corticospinal dieback is unknown. Interestingly, both aberrantly enhanced activities of CK2 and HDAC6 can impair autophagy, which is relevant to the accumulation of mutated/misfolded proteins (46,47) and hence perhaps mutant M1.

As for haploinsufficiency, why would lower spastin function cause the axon to be more vulnerable to a second disease hit? Reduced MT severing by spastin would result in longer MTs, fewer MTs and MTs that are more stable (48,49). While the changes in tubulin modifications that theoretically should arise from reduced spastin function appear to be overcome by compensatory and/or gain-of-function mechanisms, the other effects on MTs likely persist. Longer but fewer MTs would result in reduced frequency of proteins that associate with the plus and minus ends of MTs (50,51). In addition, a reduction in MT mobility would likely result from the fact that fewer MTs would be short enough to move within the axon (52). Reduced MT mobility would mean a diminished capacity of the neuron to supply tubulin subunits to the axon and also a diminished capacity to transport out of the axon MTs that have abnormally flipped their orientation. Flaws in the uniform orientation of axonal MTs provide a likely explanation for the axonal swellings because organelles would accumulate owing to their movement along misoriented MTs (53). Previous studies showed that axonal swellings resulting from spastin haploinsufficiency are comprised of cytoskeletal elements, such as neurofilaments and intertwined MTs, as well as accumulated intracellular organelles, such as mitochondria (10–12,54).

Another possibility is that haploinsufficiency has less to do with MT severing and more to do with the interaction between M1 spastin and membranous organelles (55–59). Thus, it may be that CSTs are dependent upon low levels of M1 spastin and halving these levels accounts for the axonal swellings as well as the greater vulnerability of the axon to the toxicity of the mutant M1. Such effects could be owing to abnormalities in endoplasmic reticulum (ER), endosomes or other membranous structures in the axon (55–59).

In conclusion, the present studies provide the first direct experimental support for our hypothesis on the distinct contributions of gain-of-function and loss-of-function components to the etiology of *SPG4*-HSP (17). Both the h*SPAST*-C448Y and the *Spast*-KO mouse are valuable in that each of the two isolates one of these two distinct components of the disease (Fig. 6). However, the crossbred mice are the most valuable because they display the interplay between the two components that occur in human patients and hence provide the best vertebrate model yet for testing potential therapies for the disease.

Materials and Methods
Animals

All of the animal experiments were performed in compliance with the NIH's Guide for the Care and Use of
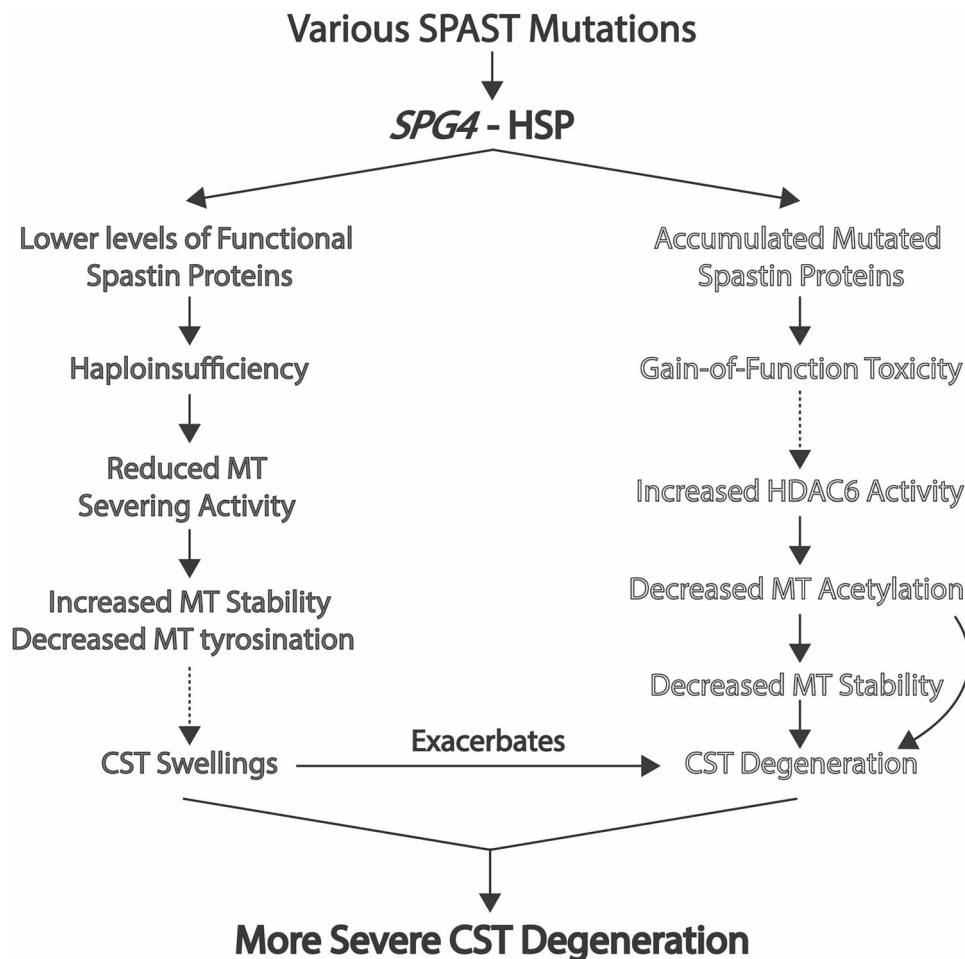
Figure 6. Hypothesis for the etiology of *SPG4*-HSP. Lower levels of spastin protein cause reduced MT severing that leads to decreasing MT mobility, which results in axonal swellings. Haploinsufficiency also leads to defective ER and endosomal functions, which also lead to axonal swellings either owing to the disruption of M1 spastin coupled membrane modeling and MT severing or to a separate mechanism not involving MT severing. On the other hand, the accumulation of mutated spastin protein manifests in increased HDAC6 activity, decreased MT acetylation and detyrosination and defective axonal transport, as well as inhibited autophagy machinery, leading to axonal dieback degeneration. We also posit that haploinsufficiency is an exacerbating factor that makes the corticospinal (indicated as CST in the schematic) tracts vulnerable to effects of the mutant spastin proteins, leading to more severe corticospinal dieback degeneration. Arrows with dotted lines indicate hypothesized mechanisms.

Laboratory Animals (National Academies Press, 2011) and were reviewed and approved by the Institutional Animal Care and Use Committee at Drexel University. The animal work for this study was carried out under the project license 1045165, protocol no. 20861 (previously 20601).

Colony generation, breeding strategy and housing

The transgenic hSPAST-C448Y mouse carries a point mutation in exon 11 of human full-length *SPAST* [*SPAST* c.1343g>a (p.Cys448Tyr), NM_014946.3, CCDS_1778.1] inserted into the Gt(ROSA)26Sor locus to allow the expression of human *SPAST* to be dependent upon Cre recombinase. We named hSPAST-C448Y$^{+/-}$ mice (human *SPAST*-C448Y heterozygous mice) h-KI-Het mice. They were generated by mating a ubiquitous Cre mouse strain with the locked *SPAST*-C448Y mice, as described in (16). The spastin KO mouse was generated using the 'knockout first allele' method (18). Briefly, spastin KO first allele

was achieved by using the trans-NIH Knockout Project obtained from the KOMP Repository, and constitutive spastin KOs were generated by deleting the floxed exon 5 in the germline using CMV-Cre Deleter mice (60,61). We named *Spast*$^{+/-}$ mice (mouse *Spast* heterozygous KO mice) m-KO-Het. Double-heterozygous mice (dHet) were initially obtained by crossbreeding m-KO-Het with h-KI-Het mice. Next, we used multiple pairs of the dHet mice to generate all the mice used in this study, including all the four genotypes: wild-type, m-KO-Het, h-KI-Het and dHet. These breeding strategies allow us to collect all of the four genotypes from the littermate mice. Mice (males and females) were group-housed as five per cage under a 12-h light/dark cycle and were divided in experimental groups: 2, 3, 6, 9, 12 and 15 months of age. Temperature and humidity were kept constant, and mice had free access to drinking water and food. For anatomical analysis, mice from each group were applied. Adult mice used for anatomical analyses were sacrificed by intraperitoneal injection of euthasol solution (150 mg/kg;

catalog 50989056912, VEDCO) and were dissected for tissue collection.

Genotyping PCR

gDNA was isolated using the EZ Tissue DNA Isolation Kit (catalog M1003, EZ Bioresearch). Around 21–28 days of age, mice are weened, and ear tissues (no larger than 2 mm) were collected and marked for subsequent digestion for genotyping analysis. The 10 ng of gDNA from *Spast* (spastin KO mice) were used to run a touchdown PCR with Taq Polymerase (Promega Go Taq Master Mix, catalog M7123) and 10 pmol/μl of each of the following primers: PLR41 (5′-AAGTCATGGCAGTCTTTCTGGCT-3′), PLR169 (5′-ATTTGCAAAAACTACTTGCTATTAAATTCC-3′), PLR89 (5′-CACATGGTGGCTCATAACCATTTA-3′). The primer pairs confirm the deletion of exon 5 and 2% agarose gel was used for electrophoresis at 80 V to visualize the PCR products: 223 base-pair band indicates the wild-type allele, while 432 base-pair band indicates the *Spast*-KO allele (Fig. 1C and D).

To determine zygosity in h*SPAST*-C448Y mice, 7.5 ng of gDNA was used to run qRT-PCR using iTaq Universal SYBR Green Supermix (catalog 1725120, BioRad). qRT-PCR was carried out with a pair of primers that are specific for the human spastin (Fw: 5′-AGCACAACTTGCTAGAATGACTG-3′; Rev: 5′-AAGTTTGAGGGCTGACGCTG-3′), as shown in Figure 1E, and IL-2 (Fw: 5′-CTAGGCCACAGAATTGAAAGATCT-3′; Rev: 5′-GTAGGTGGAAATTCTAGCATCATCC-3′) was used as a control gene with two copies to identify genotypes based on relative DNA content (Fig. 1F). The PCR reaction was carried out using the StepOne™ Real-Time PCR System (catalog 4376357, Applied Biosystems). Genotypes were detected using LinRegPCR software version 5.1.1. Only mice positive for heterozygosity with both protocols were considered as double heterozygote, dHet.

Behavioral assay: Catwalk analyses

The Catwalk assay was used to measure the gait abnormalities associated with corticospinal degeneration. The Noldus Catwalk XT automated gait analysis system consists of a glass platform above a high-resolution video camera. A fluorescent green light is reflected through the glass platform. Wherever the mouse makes contact along the platform, light is scattered, and the camera underneath acquires and transforms each scene into a digital image. The Catwalk station is also equipped with software which enables the analysis of the videos and produces a large amount of data related to hundreds of different parameters of gait, such as speed, timing and coordination. Mice were brought to an isolated behavior room 30 min before testing to allow them to acclimate. Each mouse to be tested underwent a week of training to learn the task and a week of recording for gait parameters analysis. For consistency, the training was conducted by the same person who performed the final experiment and tested the animals. Before recording, animals were allowed to habituate and crossbreed the walkway for

one to two times. Animals were individually placed on the Catwalk and were allowed to move freely in both directions. After 15–20 min, the mouse was removed from the walkway and was allowed to rest in its own cage. For detection of all parameters used in the experiments, the camera gain was set to 20 dB and the detection threshold to 0.10. All runs with a duration between 0.50 and 5.00 s to complete the walkway and a maximum speed variation of 60% were considered as successful runs. For each animal and each time point, three compliant runs were used for analysis. Compliant runs were classified for all limbs and were statistically analyzed. The software can detect >100 different parameters, including static and dynamic. Eight to 12 animals from wild-type, m-KO-Het, h-KI-Het and dHet were subjected to behavioral test at different ages: as 2, 3, 6, 9, 12 and 15 months of age, and detailed numbers of the different parameters for each genotype at each time point are summarized in Tables 1–7.

In the present study, parameters that correlate with gait deficiencies of HSP patients (23) were mainly chosen for analysis. The status of the animals was evaluated by the following five different parameters. The stand/swing duration is expressed in seconds and represents the time in which a paw is in contact (stand) or not (swing) with the glass plate; the print position is expressed in cm and measures the distance between the position of the hind paw and the previously placed front paw on the same site of the body and in the same step cycle; the step width or print width is the width (vertical direction) of the complete paw print; the base of support represents the average width in cm between either the front paws or the hind paws.

Tissue collection and preparation for anatomical analyses

Three animals per group were considered to be sufficient for anatomical analyses. Wild-type, m-KO-Het, h-KI-Het and dHet were collected at 2, 6, and 15 months of age and were sacrificed via euthanasia by intraperitoneal injection of euthasol solution at a dose of 150 mg/kg. Transcardial perfusion was performed and 0.9% NaCl (catalog BP358-212, Fisher Bioreagent) was used to rinse out blood, followed by 4% paraformaldehyde (4% PFA, catalog 19202, Electron Microscopy Sciences) in 0.1 M phosphate buffer for tissue fixation. Spinal cords were dissected out and were left in a fixative mixture of 2% PFA and 1.5% glutaraldehyde (catalog 16314, Electron Microscopy Sciences) for 1 week before being processed for plastic embedding. Cords were then washed in 0.1 M phosphate buffer and post-fixed with 1% OSO_4 (osmium tetraoxide) in phosphate buffer for 2 h, followed by sequential washes in 70, 95 and 100% ethanol and two washes in propylene oxide (PO). At this point, cords were incubated for 2 h in a mixture of Epon:PO with a 1:1 dilution and were subsequently incubated for other 2 h in Epon:PO mixture at 2:1 dilution, followed by a final incubation of about 1 h with 100% Epon. Cords were finally embedded

in fresh 100% Epon and were placed in capsules and were allowed to polymerize for 72 h in a 60°C oven.

The 1 μm sections were cut using a glass knife mounted on a microtome and were stained with toluidine blue to identify the axons on the cross-sections. Cross-sections from cervical and lumbar levels were then subjected to further analysis, as shown schematically in Figure 4A. Images of toluidine blue-stained spinal cords were taken with Axio Observer 7 Zeiss microscope with a 20×/0.8 DICII PLAN/APO objective to analyze the dorsal column. Total numbers of axons were counted using StereoInvestigator software version 11 at both cervical and lumbar levels for all the three time points. At 6 months of age of the mice, further analyses were made based on a gross histological analysis. Axonal perimeter was evaluated using ImageJ v2.0.0. Detailed numbers for each genotype at each time point are summarized in Tables 5–9.

Western blot analysis of spastin isoform expression and tubulin modifications in mouse tissues

Animals were euthanized as described before after which the spinal cord was dissected from wild-type, m-KO-Het, h-KI-Het and dHet mice at 6 months of age. Dissected tissues were homogenized in ice-cold 1× radioimmuno-precipitation assay buffer (catalog 89901, Thermo Fisher) in the presence of a phosphatase/protease inhibitor cocktail (catalogs A32953 and A32957 for protease and phosphatase inhibitors, respectively, Pierce). The 25 μg of tissues lysates were electrophoresed on 4–12% Bis/Tris gels (catalog 456-1084, BioRad) to perform sodium dodecyl sulfate-polyacrylamide gel electrophoresis. Proteins were then transferred to a PVDF membrane (catalog 1620177, BioRad), blocked with Intercept TBS Blocking Buffer (catalog 927-60001, Li-Cor) for 1 h at room temperature. Primary antibodies were diluted in 5% milk and were incubated overnight at 4°C. After rinsing with Tween-Tris-buffered saline for three times, membranes were incubated with IRDye Infrared Dye secondary antibodies 1:5000 (Li-Cor) at room temperature for 2 h, protected from light, and proteins were visualized using the Odyssey CLx Imaging system (Li-Cor). To examine the levels M1 and M85/M87 spastin isoforms, tissue lysates from spinal cords were homogenized and processed as described before and were then probed with spastin antibody 1:200 (catalog ab77144, Abcam). GAPDH (1:10000; catalog ab8245, Abcam) was used as a loading control.

Spinal cord lysates were probed with antibodies to βIII-tubulin (1:1000; catalog 801202, Biolegend), acetylated-tubulin (1:5000; catalog T6793, Sigma Aldrich) and tyrosinated-tubulin (1:2000, catalog T9028 Sigma Aldrich). GAPDH (1:10000; catalog ab8245, Abcam) was used as a loading control. Analyses were performed by evaluating the band intensities using Image studio software version 5.2.5 provided by Li-Cor. The levels of acetylated- and tyrosinated-tubulin were calculated as ratios to the level of βIII-tubulin in the same sample.

HDAC6 assay

HDAC6 activity assay was carried out according to the manufacturer's instructions using a fluorometric kit purchased from Biovision (catalog K466-100) on spinal cords lysates from wild-type, m-KO-Het, h-KI-Het and dHet mice. The assay utilizes deacetylase activity of HDAC6 toward a synthetic acetylated-peptide substrate, resulting in the release of an AFC fluorophore, which can be quantified using a conventional microplate reader. In brief, spinal cords were lysed in HDAC6 lysis buffer for 5 min on ice, centrifuged at 16000 × *g* for 10 min at 4°C, and then the supernatant was used to quantify the protein content via the Pierce bicinchoninic acid assay protein assay kit (Thermo Fischer, 23227). Five microliters of each sample were mixed with 50 μl of HDAC6 substrate mix and were incubated at 37°C for 30 min, followed by adding 10 μl of Developer to stop the reaction for 10 min at 37°C. Fluorescence was measured on a Tecan spectral plate reader at excitation/emission 380/490 nm at the end point mode at 37°C. The analysis was made using a standard curve in order to plot the fluorescence obtained from the sample (called ΔRFU) against it and thus to calculate the HDAC6 activity according to the amount of protein loaded. The results are expressed as U per mg of protein, where U stands for the amount of HDAC6 required to deacetylate 1 pmol of HDAC6 substrate per min under the assay conditions. The analysis was conducted according to the manufacturer's instructions to calculate the amount of HDAC6 activity in each sample.

Graphs and statistics

All of the statistical analyses were performed, and graphs prepared using GraphPad Prism version 8. One-way analysis of variance (ANOVA) was used followed by Tukey's honest significant difference *post hoc* test to account for multiple comparisons. At least three independent repeats were conducted for each experiment. For behavioral studies, 8–12 animals were used for each genotype tested at different ages under a strict double-blind procedure. A $P < 0.05$ was considered to be statistically significant.

Supplementary Material

Supplementary Material is available at *HMG* online.

raise the question of bias in the work reported or the conclusions, implications or opinions stated.

Funding

References

1. McDermott, C., White, K., Bushby, K. and Shaw, P. (2000) Hereditary spastic paraparesis: a review of new developments. *J. Neurol. Neurosurg. Psychiatry*, **69**, 150–160.

2. Denton, K.R., Xu, C., Shah, H. and Li, X.J. (2016) Modeling axonal defects in hereditary spastic paraplegia with human pluripotent stem cells. *Front. Biol. (Beijing)*, **11**, 339–354.

3. Hazan, J., Fonknechten, N., Mavel, D., Paternotte, C., Samson, D., Artiguenave, F., Davoine, C.S., Cruaud, C., Durr, A., Wincker, P. *et al.* (1999) Spastin, a new AAA protein, is altered in the most frequent form of autosomal dominant spastic paraplegia. *Nat. Genet.*, **23**, 296–303.

4. Burger, J., Fonknechten, N., Hoeltzenbein, M., Neumann, L., Bratanoff, E., Hazan, J. and Reis, A. (2000) Hereditary spastic paraplegia caused by mutations in the SPG4 gene. *Eur. J. Hum. Genet.*, **8**, 771–776.

5. Julien, C., Lissouba, A., Madabattula, S., Fardghassemi, Y., Rosenfelt, C., Androschuk, A., Strautman, J., Wong, C., Bysice, A., O'Sullivan, J. *et al.* (2016) Conserved pharmacological rescue of hereditary spastic paraplegia-related phenotypes across model organisms. *Hum. Mol. Genet.*, **25**, 1088–1099.

6. Newton, T., Allison, R., Edgar, J.R., Lumb, J.H., Rodger, C.E., Manna, P.T., Rizo, T., Kohl, Z., Nygren, A.O.H., Arning, L. *et al.* (2018) Mechanistic basis of an epistatic interaction reducing age at onset in hereditary spastic paraplegia. *Brain*, **141**, 1286–1299.

7. Svenson, I.K., Ashley-Koch, A.E., Gaskell, P.C., Riney, T.J., Cumming, W.J., Kingston, H.M., Hogan, E.L., Boustany, R.M., Vance, J.M., Nance, M.A. *et al.* (2001) Identification and expression analysis of spastin gene mutations in hereditary spastic paraplegia. *Am. J. Hum. Genet.*, **68**, 1077–1085.

8. Abrahamsen, G., Fan, Y., Matigian, N., Wali, G., Bellette, B., Sutharsan, R., Raju, J., Wood, S.A., Veivers, D., Sue, C.M. *et al.* (2013) A patient-derived stem cell model of hereditary spastic paraplegia with SPAST mutations. *Dis. Model. Mech.*, **6**, 489–502.

9. Solowska, J.M. and Baas, P.W. (2015) Hereditary spastic paraplegia SPG4: what is known and not known about the disease. *Brain*, **138**, 2471–2484.

10. Kasher, P.R., De Vos, K.J., Wharton, S.B., Manser, C., Bennett, E.J., Bingley, M., Wood, J.D., Milner, R., McDermott, C.J., Miller, C.C. *et al.* (2009) Direct evidence for axonal transport defects in a novel mouse model of mutant spastin-induced hereditary spastic paraplegia (HSP) and human HSP patients. *J. Neurochem.*, **110**, 34–44.

11. Tarrade, A., Fassier, C., Courageot, S., Charvin, D., Vitte, J., Peris, L., Thorel, A., Mouisel, E., Fonknechten, N., Roblot, N. *et al.* (2006) A mutation of spastin is responsible for swellings and impairment of transport in a region of axon characterized by changes in microtubule composition. *Hum. Mol. Genet.*, **15**, 3544–3558.

12. Fassier, C., Tarrade, A., Peris, L., Courageot, S., Mailly, P., Dalard, C., Delga, S., Roblot, N., Lefevre, J., Job, D. *et al.* (2013) Microtubule-targeting drugs rescue axonal swellings in cortical neurons from spastin knockout mice. *Dis. Model. Mech.*, **6**, 72–83.

13. Leo, L., Weissmann, C., Burns, M., Kang, M., Song, Y., Qiang, L., Brady, S.T., Baas, P.W. and Morfini, G. (2017) Mutant spastin proteins promote deficits in axonal transport through an isoform-specific mechanism involving casein kinase 2 activation. *Hum. Mol. Genet.*, **26**, 2321–2334.

14. Solowska, J.M., Rao, A.N. and Baas, P.W. (2017) Truncating mutations of SPAST associated with hereditary spastic paraplegia indicate greater accumulation and toxicity of the M1 isoform of spastin. *Mol. Biol. Cell*, **28**, 1728–1737.

15. Solowska, J.M., Garbern, J.Y. and Baas, P.W. (2010) Evaluation of loss of function as an explanation for SPG4-based hereditary spastic paraplegia. *Hum. Mol. Genet.*, **19**, 2767–2779.

16. Qiang, L., Piermarini, E., Muralidharan, H., Yu, W., Leo, L., Hennessy, L.E., Fernandes, S., Connors, T., Yates, P.L., Swift, M. *et al.* (2019) Hereditary spastic paraplegia: gain-of-function mechanisms revealed by new transgenic mouse. *Hum. Mol. Genet.*, **28**, 1136–1152.

17. Qiang, L., Piermarini, E. and Baas, P.W. (2019) New hypothesis for the etiology of SPAST-based hereditary spastic paraplegia. *Cytoskeleton (Hoboken)*, **76**, 289–297.

18. Lopes, A.T., Hausrat, T.J., Heisler, F.F., Gromova, K.V., Lombino, F.L., Fischer, T., Ruschkies, L., Breiden, P., Thies, E., Hermans-Borgmeyer, I. *et al.* (2020) Spastin depletion increases tubulin polyglutamylation and impairs kinesin-mediated neuronal transport, leading to working and associative memory deficits. *PLoS Biol.*, **18**, e3000820.

19. Crowley, S.T., Kataoka, K. and Itaka, K. (2018) Combined CatWalk Index: an improved method to measure mouse motor function using the automated gait analysis system. *BMC Res. Notes.*, **11**, 263.

20. Chen, Y.J., Cheng, F.C., Sheu, M.L., Su, H.L., Chen, C.J., Sheehan, J. and Pan, H.C. (2014) Detection of subtle neurological alterations by the Catwalk XT gait analysis system. *J. Neuroeng. Rehabil.*, **11**, 62.

21. Herold, S., Kumar, P., Jung, K., Graf, I., Menkhoff, H., Schulz, X., Bahr, M. and Hein, K. (2016) CatWalk gait analysis in a rat model of multiple sclerosis. *BMC Neurosci.*, **17**, 78.

22. Hamers, F.P., Koopmans, G.C. and Joosten, E.A. (2006) CatWalk-assisted gait analysis in the assessment of spinal cord injury. *J. Neurotrauma*, **23**, 537–548.

23. Serrao, M., Rinaldi, M., Ranavolo, A., Lacquaniti, F., Martino, G., Leonardi, L., Conte, C., Varrecchia, T., Draicchio, F., Coppola, G. *et al.* (2016) Gait patterns in patients with hereditary spastic paraparesis. *PLoS One*, **11**, e0164623.

24. Blackstone, C., O'Kane, C.J. and Reid, E. (2011) Hereditary spastic paraplegias: membrane traffic and the motor pathway. *Nat. Rev. Neurosci.*, **12**, 31–42.

25. Deluca, G.C., Ebers, G.C. and Esiri, M.M. (2004) The extent of axonal loss in the long tracts in hereditary spastic paraplegia. *Neuropathol. Appl. Neurobiol.*, **30**, 576–584.

26. Watson, C., Paxinos, G. and Puelles, L. (2012) Chapter 13. In Sengul, G. and Watson, C. (eds), The mouse nervous system, *Spinal Cord*. Amsterdam: Elsevier: Academic, press, pp. 424–458.

27. Solowska, J.M., D'Rozario, M., Jean, D.C., Davidson, M.W., Marenda, D.R. and Baas, P.W. (2014) Pathogenic mutation of spastin has gain-of-function effects on microtubule dynamics. *J. Neurosci.*, **34**, 1856–1867.

28. Riano, E., Martignoni, M., Mancuso, G., Cartelli, D., Crippa, F., Toldo, I., Siciliano, G., Di Bella, D., Taroni, F., Bassi, M.T. *et al.* (2009) Pleiotropic effects of spastin on neurite growth depending on expression levels. *J. Neurochem.*, **108**, 1277–1288.

29. Hammond, J.W., Cai, D. and Verhey, K.J. (2008) Tubulin modifications and their cellular functions. *Curr. Opin. Cell Biol.*, **20**, 71–76.

30. Cambray-Deakin, M.A. and Burgoyne, R.D. (1987) Acetylated and detyrosinated alpha-tubulins are co-localized in stable microtubules in rat meningeal fibroblasts. *Cell Motil. Cytoskeleton*, **8**, 284–291.

31. Li, Y., Shin, D. and Kwon, S.H. (2013) Histone deacetylase 6 plays a role as a distinct regulator of diverse cellular processes. *FEBS J.*, **280**, 775–793.

32. Boyault, C., Sadoul, K., Pabion, M. and Khochbin, S. (2007) HDAC6, at the crossroads between cytoskeleton and cell signaling by acetylation and ubiquitination. *Oncogene*, **26**, 5468–5476.

33. Errico, A., Ballabio, A. and Rugarli, E.I. (2002) Spastin, the protein mutated in autosomal dominant hereditary spastic paraplegia, is involved in microtubule dynamics. *Hum. Mol. Genet.*, **11**, 153–163.

34. Stone, M.C., Rao, K., Gheres, K.W., Kim, S., Tao, J., La Rochelle, C., Folker, C.T., Sherwood, N.T. and Rolls, M.M. (2012) Normal spastin gene dosage is specifically required for axon regeneration. *Cell Rep.*, **2**, 1340–1350.

35. Solowska, J.M., Morfini, G., Falnikar, A., Himes, B.T., Brady, S.T., Huang, D. and Baas, P.W. (2008) Quantitative and functional analyses of spastin in the nervous system: implications for hereditary spastic paraplegia. *J. Neurosci.*, **28**, 2147–2157.

36. Eira, J., Silva, C.S., Sousa, M.M. and Liz, M.A. (2016) The cytoskeleton as a novel therapeutic target for old neurodegenerative disorders. *Prog. Neurobiol.*, **141**, 61–82.

37. Baas, P.W., Rao, A.N., Matamoros, A.J. and Leo, L. (2016) Stability properties of neuronal microtubules. *Cytoskeleton (Hoboken)*, **73**, 442–460.

38. Li, L. and Yang, X.J. (2015) Tubulin acetylation: responsible enzymes, biological functions and human diseases. *Cell. Mol. Life Sci.*, **72**, 4237–4255.

39. Wang, Z., Leng, Y., Wang, J., Liao, H.M., Bergman, J., Leeds, P., Kozikowski, A. and Chuang, D.M. (2016) Tubastatin A, an HDAC6 inhibitor, alleviates stroke-induced brain infarction and functional deficits: potential roles of alpha-tubulin acetylation and FGF-21 up-regulation. *Sci. Rep.*, **6**, 19626.

40. Gal, J., Chen, J., Barnett, K.R., Yang, L., Brumley, E. and Zhu, H. (2013) HDAC6 regulates mutant SOD1 aggregation through two SMIR motifs and tubulin acetylation. *J. Biol. Chem.*, **288**, 15035–15045.

41. Selenica, M.L., Benner, L., Housley, S.B., Manchec, B., Lee, D.C., Nash, K.R., Kalin, J., Bergman, J.A., Kozikowski, A., Gordon, M.N. *et al.* (2014) Histone deacetylase 6 inhibition improves memory and reduces total tau levels in a mouse model of tau deposition. *Alzheimers Res. Ther.*, **6**, 12.

42. Zhang, L., Liu, C., Wu, J., Tao, J.J., Sui, X.L., Yao, Z.G., Xu, Y.F., Huang, L., Zhu, H., Sheng, S.L. *et al.* (2014) Tubastatin A/ACY-1215 improves cognition in Alzheimer's disease transgenic mice. *J. Alzheimers Dis.*, **41**, 1193–1205.

43. White, M.A., Kim, E., Duffy, A., Adalbert, R., Phillips, B.U., Peters, O.M., Stephenson, J., Yang, S., Massenzio, F., Lin, Z. *et al.* (2018) TDP-43 gains function due to perturbed autoregulation in a Tardbp knock-in mouse model of ALS-FTD. *Nat. Neurosci.*, **21**, 552–563.

44. Kanaan, N.M., Morfini, G.A., LaPointe, N.E., Pigino, G.F., Patterson, K.R., Song, Y., Andreadis, A., Fu, Y., Brady, S.T. and Binder, L.I. (2011) Pathogenic forms of tau inhibit kinesin-dependent axonal transport through a mechanism involving activation of axonal phosphotransferases. *J. Neurosci.*, **31**, 9858–9868.

45. Eshraghi, M., Karunadharma, P.P., Blin, J., Shahani, N., Ricci, E.P., Michel, A., Urban, N.T., Galli, N., Sharma, M., Ramirez-Jarquin, U.N. *et al.* (2021) Mutant Huntingtin stalls ribosomes and represses protein synthesis in a cellular model of Huntington disease. *Nat. Commun.*, **12**, 1461.

46. Yan, J. (2014) Interplay between HDAC6 and its interacting partners: essential roles in the aggresome-autophagy pathway and neurodegenerative diseases. *DNA Cell Biol.*, **33**, 567–580.

47. Watabe, M. and Nakaki, T. (2011) Protein kinase CK2 regulates the formation and clearance of aggresomes in response to stress. *J. Cell Sci.*, **124**, 1519–1532.

48. Kuo, Y.W., Trottier, O. and Howard, J. (2019) Predicted effects of severing enzymes on the length distribution and Total mass of microtubules. *Biophys. J.*, **117**, 2066–2078.

49. Vemu, A., Szczesna, E., Zehr, E.A., Spector, J.O., Grigorieff, N., Deaconescu, A.M. and Roll-Mecak, A. (2018) Severing enzymes amplify microtubule arrays through lattice GTP-tubulin incorporation. *Science*, **361**:768–781.

50. Matamoros, A.J. and Baas, P.W. (2016) Microtubules in health and degenerative disease of the nervous system. *Brain Res. Bull.*, **126**, 217–225.

51. Akhmanova, A. and Steinmetz, M.O. (2015) Control of microtubule organization and dynamics: two ends in the limelight. *Nat. Rev. Mol. Cell. Biol.*, **16**, 711–726.

52. Baas, P.W., Karabay, A. and Qiang, L. (2005) Microtubules cut and run. *Trends Cell Biol.*, **15**, 518–524.

53. Baas, P.W. and Mozgova, O.I. (2012) A novel role for retrograde transport of microtubules in the axon. *Cytoskeleton (Hoboken)*, **69**, 416–425.

54. Denton, K.R., Lei, L., Grenier, J., Rodionov, V., Blackstone, C. and Li, X.J. (2014) Loss of spastin function results in disease-specific axonal defects in human pluripotent stem cell-based models of hereditary spastic paraplegia. *Stem Cells*, **32**, 414–423.

55. Chang, C.L., Weigel, A.V., Ioannou, M.S., Pasolli, H.A., Xu, C.S., Peale, D.R., Shtengel, G., Freeman, M., Hess, H.F., Blackstone, C. *et al.* (2019) Spastin tethers lipid droplets to peroxisomes and directs fatty acid trafficking through ESCRT-III. *J. Cell Biol.*, **218**, 2583–2599.

56. Papadopoulos, C., Orso, G., Mancuso, G., Herholz, M., Gumeni, S., Tadepalle, N., Jungst, C., Tzschichholz, A., Schauss, A., Honing, S. *et al.* (2015) Spastin binds to lipid droplets and affects lipid metabolism. *PLoS Genet.*, **11**, e1005149.

57. Connell, J.W., Allison, R.J., Rodger, C.E., Pearson, G., Zlamalova, E. and Reid, E. (2020) ESCRT-III-associated proteins and spastin

inhibit protrudin-dependent polarised membrane traffic. *Cell. Mol. Life Sci.*, **77**, 2641–2658.

58. Allison, R., Lumb, J.H., Fassier, C., Connell, J.W., Ten Martin, D., Seaman, M.N., Hazan, J. and Reid, E. (2013) An ESCRT-spastin interaction promotes fission of recycling tubules from the endosome. *J. Cell Biol.*, **202**, 527–543.

59. Park, S.H., Zhu, P.P., Parker, R.L. and Blackstone, C. (2010) Hereditary spastic paraplegia proteins REEP1, spastin, and atlastin-1 coordinate microtubule interactions with the tubular ER network. *J. Clin. Invest.*, **120**, 1097–1110.

60. Brill, M.S., Kleele, T., Ruschkies, L., Wang, M., Marahori, N.A., Reuter, M.S., Hausrat, T.J., Weigand, E., Fisher, M., Ahles, A. *et al.* (2016) Branch-specific microtubule destabilization mediates axon branch loss during neuromuscular synapse elimination. *Neuron*, **92**, 845–856.

61. Testa, G., Schaft, J., van der Hoeven, F., Glaser, S., Anastassiadis, K., Zhang, Y., Hermann, T., Stremmel, W. and Stewart, A.F. (2004) A reliable lacZ expression reporter cassette for multipurpose, knockout-first alleles. *Genesis*, **38**, 151–158.

62. Fonknechten, N., Mavel, D., Byrne, P., Davoine, C.S., Cruaud, C., Bonsch, D., Samson, D., Coutinho, P., Hutchinson, M., McMonagle, P. *et al.* (2000) Spectrum of SPG4 mutations in autosomal dominant spastic paraplegia. *Hum. Mol. Genet.*, **9**, 637–644.